The role of eastern Siberian snow and soil moisture anomalies in quasi-biennial persistence of the Arctic and North Atlantic Oscillations

R. J. Allen[1] and C. S. Zender[1]

Received 8 November 2010; revised 8 April 2011; accepted 8 June 2011; published 31 August 2011.

[1] Variations in the Arctic Oscillation (AO) and its regional manifestation, the North Atlantic Oscillation (NAO), generate much of the nonseasonal variability in the winter climate over the Northern Hemisphere midlatitudes. Despite being an internal mode of the atmosphere, the Arctic and North Atlantic Oscillations (N/AO) exhibit a slightly red spectrum, varying on quasi-biennial (2–3 years) and quasi-decadal time scales. Such low-frequency variability is likely due to the coupling of the atmosphere to boundary conditions and/or external forcings. Here we show that Eurasian snow cover, particularly over eastern Siberia (ESB), exhibits quasi-biennial persistence similar to the N/AO. Furthermore, the snow-AO mechanism operates on quasi-biennial timescales, with fall ESB snow cover significantly related to vertically propagating Rossby wave activity and the N/AO for the next two to three winters. On the basis of land surface model simulations from the Global Land Data Assimilation System (GLDAS), the interseasonal carryover of ESB snow is related to soil moisture anomalies and an evaporation-convection feedback. These findings suggest quasi-biennial persistence of the N/AO is partly due to land surface forcing in the form of both ESB snow and soil moisture anomalies.

Citation: Allen, R. J., and C. S. Zender (2011), The role of eastern Siberian snow and soil moisture anomalies in quasi-biennial persistence of the Arctic and North Atlantic Oscillations, *J. Geophys. Res.*, *116*, D16125, doi:10.1029/2010JD015311.

1. Introduction

[2] The dominant mode of extratropical Northern Hemisphere (NH) wintertime atmospheric circulation variability and its regional manifestation in the North Atlantic are referred to as the Arctic Oscillation (AO) [*Thompson and Wallace*, 1998] and the North Atlantic Oscillation (NAO) [*Wallace and Gutzler*, 1981], respectively. Their spatial structure is characterized by anomalous sea level pressure (SLP) of one sign throughout the Arctic, with anomalies of the opposite sign centered over the Azores and, for the AO, over the North Pacific. These circulation patterns have a strong impact on wintertime surface temperature, precipitation, and storminess over much of North America and Eurasia [e.g., *Hurrell*, 1995; *Thompson and Wallace*, 2000].

[3] Although both appear to be fundamental, internal modes of the atmosphere with a timescale on the order of a week [e.g., *Feldstein*, 2000], proxy records [*Cook and D'Arrigo*, 2002; *Jones et al.*, 2001] and instrumental data [*Schneider and Schonwiese*, 1989; *Saito and Cohen*, 2003] show the NAO and AO (N/AO) exhibit significant low-frequency variability, with periods of prolonged positive or negative N/AO index values. The power spectrum of the N/AO is slightly red, with significant power at 7–25 year timescales [*Rogers*, 1984; *Cook et al.*, 1998], and at quasi-biennial timescales of 2–3 years [*Schneider and Schonwiese*, 1989; *Stephenson et al.*, 2000; *Cook and D'Arrigo*, 2002].

[4] There is increasing evidence that the low-frequency N/AO variability comes from coupling with other components of the climate system, such as tropical [*Hoerling et al.*, 2001; *Hurrell et al.*, 2004] and extratropical [*Rodwell et al.*, 1999; *Robertson et al.*, 2000] sea surface temperatures (SSTs), as well as external forcings, such as greenhouse gases (GHGs) [*Shindell et al.*, 1999; *Fyfe et al.*, 1999; *Gillett et al.*, 2003; *Osborn*, 2004; *Miller et al.*, 2006]. Recent studies also show Eurasian (EA) snow cover affects the AO, influencing its phase, strength and interannual variability [e.g., *Cohen and Entekhabi*, 1999; *Gong et al.*, 2002; *Saito and Cohen*, 2003; *Cohen and Barlow*, 2005]. Observations also support a snow-AO mechanism, whereby anomalously high EA snow cover in autumn results in an increase in upward stationary Rossby wave activity, which slows the polar vortex and increases high-latitude geopotential heights. This anomaly then propagates downward through the troposphere, resulting in a negative AO-like response at the surface during winter [*Saito et al.*, 2001; *Cohen et al.*, 2007; *Hardiman et al.*, 2008; *Cohen et al.*, 2010]. Moreover, EA snow also exhibits spectral peaks at the quasi-biennial and quasi-decadal timescale, similar to the preferred periods of N/AO oscillation [*Ye*, 2001; *Saito and Cohen*, 2003]. *Bojariu and Gimeno* [2003] suggest the existence of a snow-NAO persistence mechanism, whereby winter/spring NAO circu-

[1]Department of Earth System Science, University of California, Irvine, California, USA.

0148-0227/11/2010JD015311

lation anomalies influence snow cover, which in turn affect the NAO in summer/fall.

[5] In this paper, we show that quasi-biennial (2–3 year) N/AO persistence is related to October snow cover anomalies in eastern Siberia (ESB). Moreover, the snow-AO mechanism operates on the same quasi-biennial timescale. Although a high fall snow cover anomaly does not persist through the summer, we show that summertime soil moisture anomalies provide a memory of snow mass. This paper is organized as follows: section 2 describes our data sets and the methods employed. Results are presented in section 3, followed by conclusions in section 4.

2. Data and Methods

[6] Monthly snow cover fraction data (1° × 1°) from 1972 to 2007 comes from the National Oceanographic and Atmospheric Administration (NOAA) satellite data set, based primarily on visible band imagery (see http://climate.rutgers.edu/snow cover/index.php). Atmospheric data, such as sea level pressure (SLP), geopotential heights (Z) and winds, comes from monthly and daily National Centers for Environmental Prediction/National Center for Atmospheric Research (NCEP/NCAR) reanalysis (R1) data [*Kalnay et al.*, 1996].

[7] The global soil moisture data bank has soil moisture observations for over 600 stations, including the former Soviet Union, Mongolia, and China [*Robock et al.*, 2000]. However, few stations exist in Siberia; those that do possess limited record lengths and generally have many missing data (e.g., data only exists for the growing season). Therefore, because of the lack of long-term, Eurasia-wide soil moisture observations, we use 1979–2007 1° × 1° monthly soil moisture data from four offline (i.e., not coupled to the atmosphere) land surface models (LSMs) driven by the Global Land Data Assimilation System (GLDAS) [*Rodell et al.*, 2004] (see http://disc.gsfc.nasa.gov/hydrology). The GLDAS data product consists of land surface states (e.g., soil moisture) and surface energy fluxes (e.g., evapotranspiration) driven by four LSMs, including Mosaic (MOS), Noah, the Community Land Model 2.0 (CLM), and the Variable Infiltration Capacity (VIC). Each LSM is forced by observation-based meteorological fields including precipitation, near-surface winds, near-surface temperature, near-surface specific humidity, downward shortwave and longwave radiation, and surface pressure. In addition to soil moisture, we also use the following GLDAS output fields: snow water equivalent, surface temperature, snowmelt, snow and rain rate, and evapotranspiration.

[8] Several studies have shown that the GLDAS soil moisture data is generally in good agreement with observations, but improvement is still needed. *Berg et al.* [2005] found that soil moisture estimates using Mosaic with bias-corrected hydrometeorological forcing data are in good agreement with in situ measurements, and in general statistical agreement with satellite observations of surface soil moisture wetness. More recently, *Zhang et al.* [2008] found the GLDAS subsurface soil moisture data are very consistent with the observations in Illinois with respect to the annual cycle. Results also showed that monthly and interannual variations of the GLDAS soil moisture data are in good agreement with the observations.

[9] Despite the poor quality of soil moisture from most reanalyses [e.g., *Kanamitsu et al.*, 2002; *Li et al.*, 2005; *Lu et al.*, 2005], we also briefly look at soil moisture from NCEP/NCAR reanalysis, NCEP-Department of Energy (DOE) Atmospheric Model Intercomparison Project (AMIP) II reanalysis (R2) [*Kanamitsu et al.*, 2002], the European Centre for Medium-Range Weather Forecasts (ECMWF) reanalysis (ERA-40) [*Uppala et al.*, 2005] and the Japanese 25 year reanalysis (JRA-25) [*Onogi et al.*, 2007].

[10] Thermal forcings have been shown to amplify orographically forced stationary waves [*Ringler and Cook*, 1999] and both observational [*Saito et al.*, 2001; *Cohen et al.*, 2007] and modeling [*Gong et al.*, 2003; *Fletcher et al.*, 2009; *Allen and Zender*, 2010] studies have associated upward propagating Rossby waves with anomalously high Siberian snow. In this paper, we use the vertical component of the wave activity flux (WAF) to quantify the upward propagation of planetary waves [*Plumb*, 1985]:

$$\mathrm{WAF} = \Omega \cos(\phi) \sin(\phi) S^{-1} \left[v'T' - \frac{1}{2\Omega R_e \sin(2\phi)} \frac{\partial}{\partial \lambda} (T'\Phi') \right], \tag{1}$$

where variables represent their standard meteorological values, R_e is mean radius of the earth, λ is longitude, ϕ is latitude, Ω is the angular velocity of rotation, S is static stability and primes denote deviations from the zonal mean. WAF is useful for localizing in longitude and latitude the source of vertically propagating stationary Rossby waves and is proportional to the vertical component of the often-used quasi-geostrophic Eliassen-Palm (EP) flux [*Edmon et al.*, 1980]. WAF is calculated on the basis of daily NCEP/NCAR reanalysis data and zonally averaged from 40°N to 80°N.

[11] The AO is calculated as the leading principal component of sea level pressure or geopotential height poleward of 20°N. The positive AO phase is defined to have low high-latitude SLP/Z and high midlatitude SLP/Z. The NAO is estimated as the difference in SLP/Z averaged over a southern (30°N–50°N, 80°W–20°E) minus a northern (60°N–80°N, 80°W–20°W) domain [e.g., *Hurrell et al.*, 2004]. The NAO, therefore, has the same spatial orientation as the AO, with its positive phase possessing low SLP/Z in the northern North Atlantic and high SLP/Z in the southern North Atlantic.

[12] Our primary analysis involves lagged correlations, where, for example, October snow cover is correlated with next five wintertime AOs (i.e., snow cover is lagged). All data is detrended before correlation analysis. Area-wide correlations are based on single time series, with cosine latitude area-weighting applied to each grid cell. Statistical significance of correlations, r, are based on a Student's t test, with the t value calculated according to $r\sqrt{(n-2)(1-r^2)^{-1}}$, where n is the number of years. The effective time between independent samples is estimated from the autoregressive properties of both time series [*Livezey*, 1999]:

$$\tau = 1 + 2 \times \sum_{i=1}^{N} \left(1 - \frac{i}{n}\right) \rho_{i,1} \rho_{i,2}, \tag{2}$$

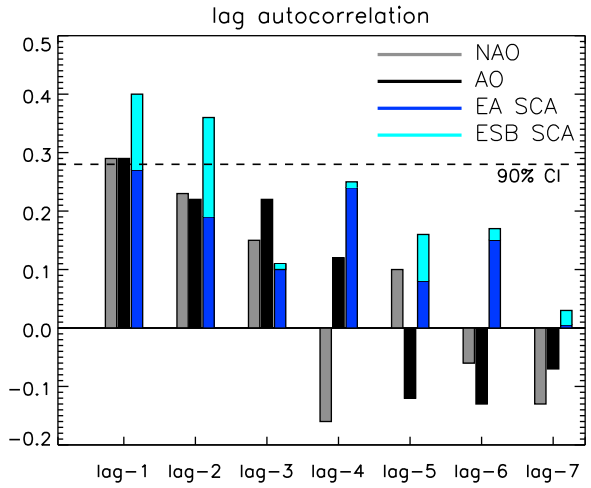

Figure 1. The 1972–2007 lag autocorrelations for October Eurasian (30°–90°N, 0°–180°E) and eastern Siberian (ESB, 40°–90°N, 90°–140°E) snow cover area (SCA) and the December-March Arctic Oscillation (AO) and North Atlantic Oscillation (NAO) at 500 hPa. Also included is the 90% confidence interval (dashed line).

where $N \leq n$, $\rho_{i,1}$ is the lag i autocorrelation for variable 1, and $\rho_{i,2}$ is the lag i autocorrelation for variable 2. The ensure a reasonably large sample size for all N lag autocorrelations, we use $N = n/2$ (~15 values for the GLDAS analysis). From τ, the effective number of degrees of freedom are n/τ. To evaluate field significance of a spatial correlation, we calculate the percentage of the given area with locally significant tests and compare this test statistic to a null distribution based on a moving-block bootstrap [*Chen*, 1982; *Wilks*, 1995; *Livezey*, 1999].

[13] In addition, we perform a multivariate principal component analysis (PCA) [*Wilks*, 1995], which produces empirical orthogonal functions successively maximizing the joint variance of the variables. Such an analysis accounts for correlations both between and among the variables at each location. Before performing PCA, each field is interpolated to 2.5° resolution, spatially smoothed using a nine-point filter, and area weighted by the cosine of latitude.

[14] Because of the nonuniform soil layer depths in the LSMs, we scale the soil moisture to the top 1 m. This is done by summing the soil moisture of each layer with accumulated depth ≤1 m; if the ith soil layer yields an accumulated depth >1 m, its soil moisture is scaled by the fraction it contributes to the top 1 m. For example, VIC contains three soil layers of depths 0–0.1, 0.1–1.6, and 1.6–1.9 m. To get the 1 m soil moisture, we add the first layer's soil moisture and 60% of the second layer's (i.e., 0.9/1.5).

3. Results

3.1. Snow-N/AO Relationship

[15] Figure 1 shows lag autocorrelations for October Eurasian (EA) (30°N–90°N; 0°–180°E) snow cover area (SCA) and the December-March (DJFM) AO and NAO at 500 hPa (similar, but somewhat weaker autocorrelations exist using the surface-based N/AO). Each feature positive autocorrelations out to lag 3, corresponding to 3 years of persistence. Figure 1 also shows that the eastern domain (40°N–90°N, 90°E–140°E), which we refer to as eastern Siberia (ESB), possess much stronger SCA autocorrelations, particularly at lag 1 (r_1 = 0.40) and lag 2 (r_2 = 0.36). Furthermore, the largest EA and ESB SCA persistence occurs in October (the lag 1 ESB SCA autocorrelation is 0.13 for September and 0.03 for November), which corresponds to the month the snow-AO relationship is most significant (not shown). On the basis of this analysis, subsequent plots involving snow cover feature October ESB SCA. Results are generally similar, but weaker, when EA SCA is used.

[16] Figure 2 shows monthly lag correlations between October eastern Siberian SCA and polar cap (>60°N) geopotential height (ZPC), zonal winds at 60°N (U60N), the NAO and AO for the subsequent five winters. Anomalously high October ESB SCA is associated with anomalously high winter/early spring (December-March) ZPC throughout the atmosphere in the first 3 years, with less significant correlations in the subsequent 2 years. A similar relationship exists for U60N, with high October ESB SCA associated with reduced U60N in both the current, and next two to three winters. Higher ZPC and reduced U60N is consistent with the negative AO phase, which also exhibits significant (negative) correlations with October ESB SCA in each of the three subsequent winters, and less significant correlations in the next two. A similar relationship exists for the NAO, with significant negative correlations up to the third winter. This analysis suggests anomalously high ESB October SCA is associated with a negative N/AO not only for the subsequent winter, but for the next two to three winters.

[17] As mentioned in the Introduction, the snow-AO relationship involves a snow-induced increase in upward stationary Rossby wave activity, which slows the polar vortex and increases high-latitude geopotential heights [*Saito et al.*, 2001; *Gong et al.*, 2003; *Cohen et al.*, 2007; *Fletcher et al.*, 2009]. Figure 3 shows this relationship in terms of the lag correlation between October ESB SCA and daily WAF 40°N–80°N for the current fall/subsequent winter (lag 0/lag 1), and separately for the following two falls/winters. Similar to *Cohen et al.* [2007], anomalously high October ESB SCA is associated with upward Rossby wave activity: weakly in late fall and then very strongly in early winter, where stratospheric correlations reach 0.5 throughout December. Moreover, Figure 3 shows that this relationship exits in subsequent winters, consistent with the quasi-biennial persistence of October ESB SCA (Figure 1). Anomalous upward WAF occurs in the subsequent year (lag 1/lag 2), where correlations once again approach 0.5 in late December, and in the next year, although the relationship is somewhat weaker and confined to early December. The strong snow-WAF relationship in the first three fall/winters (lag 0 through lag 3) is consistent with the strong (negative) snow-AO relationship in Figure 2.

3.2. Snow-Soil Moisture

[18] What causes the 2–3 year persistence of EA/ESB October snow cover? Figure 4 shows, via spatial lag correlations, that anomalously high October SCA generally persists to the subsequent late spring/early summer (AMJ), particularly over eastern EA, including the Tibetan Plateau, northeastern China, and central and eastern Russia. This is

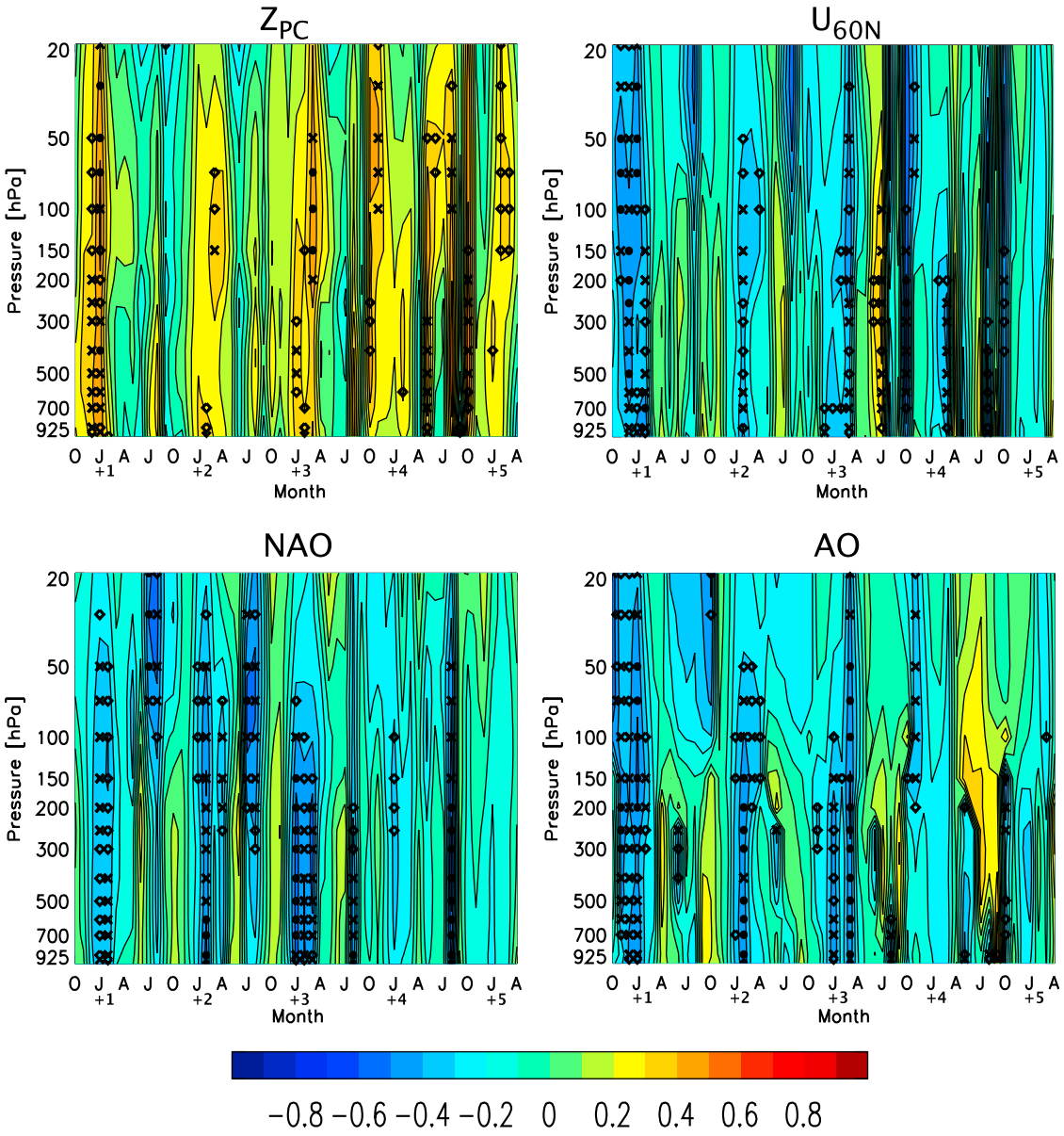

Figure 2. The 1972–2007 lag correlations between October ESB SCA and monthly (top left) Z_{PC}, (top right) U60N, (bottom left) NAO, and (bottom right) AO for the subsequent five winters. Lag correlations are plotted from October at lag 0 through April at lag 5, with the *i*th lag denoted with "+(*i*." Symbols represent significance based on Student's *t* test, accounting for the effective time between independent samples, at the 90% (diamonds), 95% (crosses), and 99% (dots) confidence levels.

consistent with the notion that high SCA will increase the surface albedo [*Yasunari et al.*, 1991], reducing the net solar radiation at the surface and hence surface temperatures, creating a situation favorable for snow persistence. Figure 4 shows that the October SCA anomaly, however, does not persist through the subsequent August, when nearly all (except over the Tibetan Plateau) of the October snow anomaly has melted. Nonetheless, consistent with the large lag 1 autocorrelation of ESB SCA (Figure 1; $r_1 = 0.40$), the subsequent October features high SCA over eastern Siberia, particularly over the Tibetan Plateau and central and eastern Russia. Figure 4 (bottom) shows that a similar relationship exists for the following October (lag 2).

[19] Because the snow anomaly does not persist through the summer, yet reappears the following October, a mechanism must exist that provides the climate system with a memory of the October snow anomaly. Such memory may come from the ocean, given its large heat capacity and longer timescales of circulation (relative to the atmosphere). The snow-AO relationship itself may also play a role, as *Bojariu and Gimeno* [2003] showed that in winter and early spring, NAO type atmospheric circulations influence the extent of snow cover, which in turn affects the atmosphere in the late spring, summer and early autumn. GCM experiments [e.g., *Yeh et al.*, 1983; *Barnett et al.*, 1989; *Yasunari et al.*, 1991] suggest a summertime snow-hydrological feedback, particularly over eastern Siberia [*Matsumura et al.*, 2010].

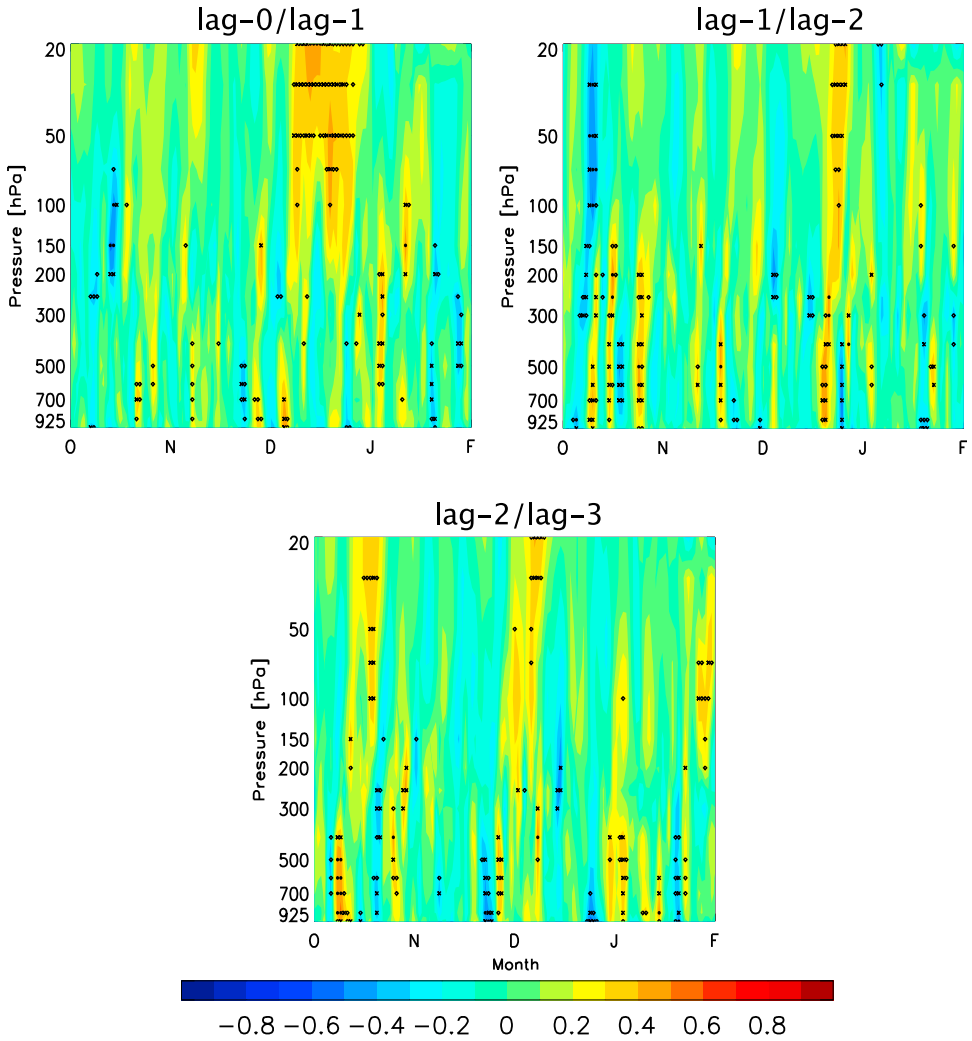

Figure 3. The 1972–2007 lag correlations between October ESB SCA and daily wave activity flux (WAF) 40°N–80°N for the current (lag 0) fall/subsequent (lag 1) winter and for the next two falls/winters (October-February). Symbols represent significance as in Figure 2.

The mechanism involves a large winter/spring snow anomaly (which itself persists because of high albedo and reduced surface solar absorption), which leads to a large summer soil moisture anomaly, and subsequently to more evaporation/latent heating. This results in (1) depressed temperatures and (2) more precipitation, which acts to sustain the soil moisture anomaly through an evaporation-convection feedback, recycling water between land and atmosphere. Both of these conditions are favorable for snow in the subsequent fall.

[20] Several observation-based studies have showed most of Eurasia, including eastern Siberia, possesses a large precipitation recycling ratio, indicating much of the local precipitation originates from evapotranspiration from that same region. For example, *Dirmeyer and Brubaker* [2007] used the quasi-isentropic back-trajectory method, which traces the air contributing to a precipitation event backward in time to map the most recent evaporative sources of the water vapor contributing to that event, and found relatively high precipitation recycling over eastern Siberia, particularly for June-August (JJA). Using a product similar to GLDAS, *Dirmeyer et al.* [2009] also found evidence that land-atmosphere hydrological feedbacks exist over Siberia during JJA, specifically, that soil moisture controls evaporation rates, that the climate regime allows anomalies in soil moisture to persist, and that hydrologic anomalies are reinforced through recycling. Similarly, *van der Ent et al.* [2010] showed that continental moisture feedback accounts for 70%–90% of the precipitation falling in an area ranging from eastern Europe to the Pacific Ocean and from the Arctic Ocean to north of India. These studies all suggest an eastern Siberian snow-soil moisture anomaly may be sustained through the summer by an evaporation-convection feedback mechanism.

[21] Figure 5 shows a variety of seasonal spatial correlations based on the Variable Infiltration Capacity LSM driven by GLDAS. All variables shown are model predicted, except snow cover area (SCA), which is based on NOAA satellite observations (rain rate is derived from observed precipitation, which are likely equal for most locations during JJA). Figures 5a and 5b shows the relationship between the prior October NOAA SCA and the subsequent winter (January-March, JFM) snow water equivalent (SWE). A positive relationship exists, primarily for eastern

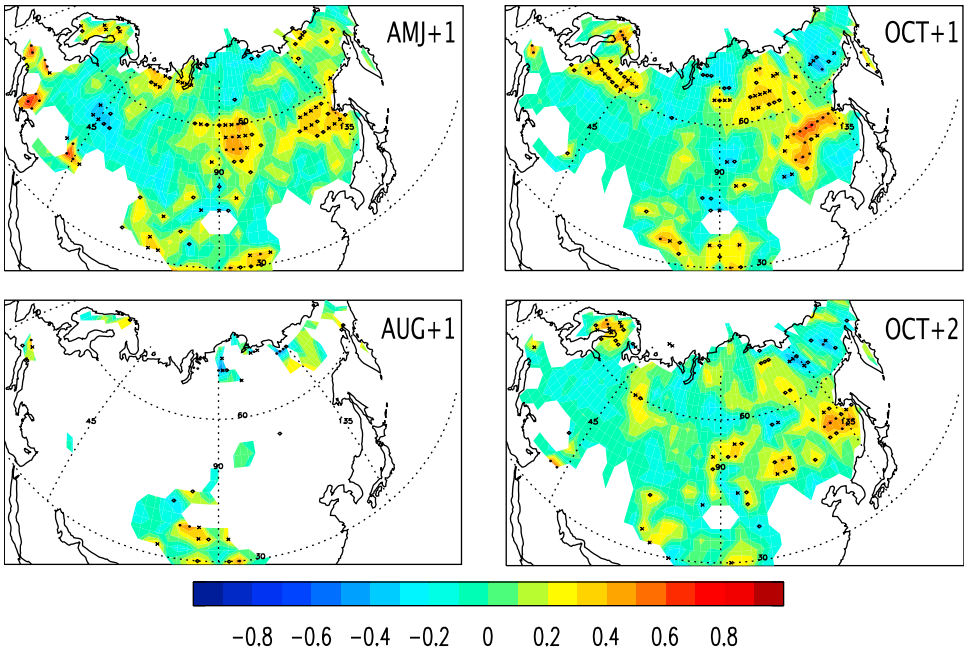

Figure 4. The 1972–2007 lag SCA correlations between October and the subsequent (lag 1) April-June (AMJ+1), August (AUG+1), and October (OCT+1) and the lag 2 October (OCT+2). Data have been interpolated to 2.5° resolution. Symbols represent significance as in Figure 2.

Siberia, where ~7% of ESB possess significant positive correlations. A moving-block bootstrap procedure [*Wilks*, 1995] was used to determine the field significance of this relationship is 90%; a somewhat stronger relationship exists if the prior September-November (SON) SCA is used (Table 1). High JFM SWE, in turn, is associated with high soil water (SW) of the top 1 m for the subsequent summer (JJA) for nearly all of the Asian continent. Although this relationship is stronger in western Siberia, it is also significant at the 99% confidence level for ESB. Similar results are obtained with spring (March-May, MAM) SWE and JJA SW (Table 1). Figure 5 also shows that high JJA SW is associated with high JJA evapotranspiration (ET) and a high JJA rain rate (RR), consistent with the soil moisture evaporation-convection feedback. The negative ET correlations in northern Siberia are due to a combination of snow and frozen ground in early summer. Figure 5e shows that high JJA SW is also associated with high October snow rates (and SWE), particularly over the Tibetan Plateau, north central and eastern Siberia, and north of the Black and Caspian seas (Ukraine and Kazakhstan). These areas generally overlap with those of high JFM SWE-JJA SW, high JJA SW-ET/RR and closely correspond to the same areas of October SCA persistence (Figure 4). Furthermore, the bottom right panel shows high JJA SW is associated with high October NOAA SCA in eastern Siberia. Although the field significance of this last relationship is less than 90% (Table 1), this analysis suggests quasi-biennial persistence of October ESB SCA is related to soil moisture anomalies and the evaporation/convection feedback.

[22] Similar results are generally obtained with the other GLDAS models. For example, Table 1 shows that the ESB JFM SWE versus JJA SW relationship is significant at the 99% confidence level for VIC, Noah, and MOS (but not for CLM). The evaporation-convection feedback (JJA SW-JJA RR and JJA SW-JJA RR) is also significant for the four GLDAS models, as are the JJA SW versus SON SWE/SR relationships (but not JJA SW-SON/October SCA). The JJA SW-JJA T_s relationship is also generally consistent with the snow-hydrological feedback, with high SW associated with low T_s, particularly for MOS. This mechanism, however, is weaker than the evaporation-convection feedback. The CLM model is somewhat different in that it has a weak winter/spring SWE-summer SW relationship (although the other relationships are similar). This weaker relationship also exists if soil water is estimated using CLM's entire 3.432 m soil column. The low winter SWE-summer SW CLM correlations may be due to weak hydraulic conductivity, inhibiting the infiltration of melting snow water. However, CLM is the lone GLDAS model that does not possess quasi-biennial ESB October SWE persistence. The ESB area average lag 1 autocorrelation of October SWE is 0.59 in VIC, 0.48 in Noah and 0.20 in MOS, but −0.01 in CLM. We note that CLM 2.0 is nearly 10 years old; the newest version (4.0) includes several improvements, such as a soil evaporation parameterization and the Snow and Ice Aerosol Radiation (SNICAR) snow model [*Flanner and Zender*, 2005].

[23] Table 2 shows that the GLDAS correlation analysis is generally similar if the topsoil level (as opposed to the top 1 m) is used. In fact, most relationships are somewhat stronger when using the topsoil level, including the correlation between SW and T_s, RR and ET. However, the wintertime SWE-summertime SW is generally weaker (except for CLM). This suggests the importance of deeper soil moisture in the snow-hydrological feedback; with high winter/spring SWE, the snowmelt SW anomaly is communicated deep within the soil column, which subsequently

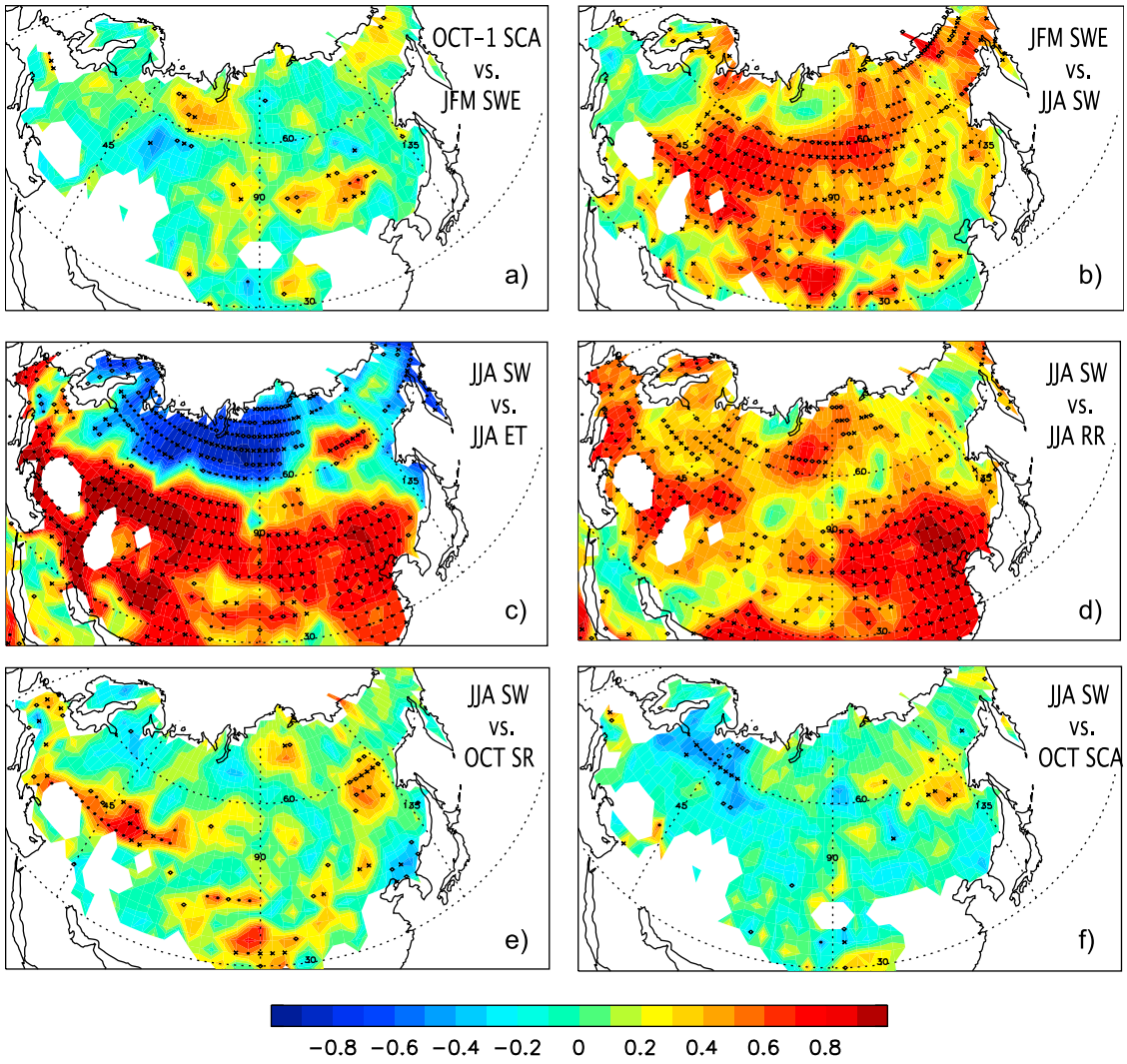

Figure 5. Spatial Variable Infiltration Capacity (VIC) correlations between (a) the prior October SCA and the subsequent January-March (JFM) snow water equivalent (SWE), (b) JFM SWE and June-August (JJA) soil water (SW), (c) JJA SW and JJA evapotranspiration (ET), (d) JJA SW and JJA rain rate (RR), (e) JJA SW and October snow rate (SR), and (f) JJA SW and October NOAA SCA. Data have been interpolated to 2.5° resolution. Symbols represent significance as in Figure 2.

Table 1. Eastern Siberia Area-Weighted Percentage of Significant Positive (P) and Negative (N) Seasonal Hydrological Correlations for the Four GLDAS Land Surface Models[a]

	VIC		Noah		MOS		CLM	
	P	N	P	N	P	N	P	N
SON-1 SCA/JFM SWE	**9.1***	0.0	4.5	0.4	**7.2***	0.0	**6.1**	0.4
October-1 SCA/JFM SWE	**6.6**	0.7	4.0	1.2	3.0	1.3	5.1	0.7
JFM SWE/JJA SW	**39.8****	0.0	**28.9****	0.5	**26.0****	0.0	5.2	**7.1**
MAM SWE/JJA SW	**30.7***	0.0	**22.8***	0.0	**22.5***	0.0	2.5	5.1
JJA SW/JJA RR	**35.1****	0.0	**37.9****	0.0	**36.4****	0.0	**74.3****	0.0
JJA SW/JJA ET	**25.1****	**13.2***	**17.7**	**12.3**	**31.2****	**20.4****	**51.0****	0.0
JJA SW/JJA T_s	0.1	**9.4**	0.5	**15.4***	0.6	**32.9****	0.6	**18.7****
JJA SW/SON SR	**8.0***	0.0	**6.3**	0.0	**8.2***	0.0	**18.1****	0.0
JJA SW/SON SWE	**10.6***	0.0	**11.0***	0.6	**7.6***	0.0	**13.6****	1.0
JJA SW/SON SCA	4.2	0.6	1.8	1.6	2.8	1.1	2.9	1.0
JJA SW/October SCA	2.9	0.5	1.2	2.1	1.0	1.6	4.3	2.9

[a]Soil water correlations are based on a 1 m soil layer depth. Snow cover area (SCA) is based on NOAA satellite observations. Field significance based on resampling is denoted by bold; values without an asterisk are ≥90%; those with one asterisk (*) are ≥95%, and those with two asterisks (**) are ≥99%. GLDAS, Global Land Data Assimilation System; VIC, Variable Infiltration Capacity; MOS, Mosaic; CLM, Community Land Model 2.0; SON, September, October, and November; JJA, June, July, and August; JFM, January, February, and March; MAM, March, April, and May; SWE, snow water equivalent; SW, soil water; RR, rain rate; T_s, surface temperature; SR, snow rate.

Table 2. Eastern Siberia Area-Weighted Percentage of Significant Positive (P) and Negative (N) Seasonal Hydrological Correlations for the Four GLDAS Land Surface Models[a]

	VIC		Noah		MOS		CLM	
	P	N	P	N	P	N	P	N
JFM SWE/JJA SW	**7.0**	1.3	**28.6****	0.6	**19.6****	0.6	**13.8****	3.5
MAM SWE/JJA SW	**9.5***	1.1	**21.2****	0.0	**17.5****	0.6	**12.7****	2.2
JJA SW/JJA RR	**91.7****	0.0	**73.9****	0.0	**37.1****	0.0	**86.2****	0.0
JJA SW/JJA ET	**47.8****	**14.9****	**24.4****	**11.6***	**32.2****	**21.9****	**71.8****	5.2
JJA SW/JJA T_s	0.0	**22.0****	0.6	**30.7****	0.0	**41.9****	0.6	**44.9****
JJA SW/SON SR	**16.2****	0.0	**10.2***	0.0	**7.9***	0.0	**22.0****	0.0
JJA SW/SON SWE	**8.3***	0.0	**9.9***	0.0	**7.0**	0.4	**15.6****	0.4
JJA SW/SON SCA	0.2	0.9	0.6	2.0	4.4	2.0	0.7	1.6
JJA SW/October SCA	1.5	1.8	0.8	3.6	1.6	5.2	0.4	2.3

[a]Soil water correlations are based on each model's top layer soil water. Top layer soil depth is 0.1 m for VIC and Noah, 0.02 m for MOS, and 0.018 for CLM. Field significance based on resampling is denoted by bold; values without an asterisk are ≥90%; those with one asterisk (*) are ≥95%, and those with two asterisks (**) are ≥99%.

allows the soil moisture anomaly to persist through the summer.

[24] Table 3 shows that the winter/spring SWE versus summer SW relationship, and the summer SW versus SON SWE relationship based on the four major reanalyses is much weaker and generally inconsistent between the four reanalyses. For example, the MAM SWE-JJA SW relationship possesses more significant positive ESB correlations (on an area-weighted basis) for both R1 and R2, but more significant negative correlations for ERA-40 and JRA-25 (in disagreement with GLDAS). The reanalyses, however, consistently show a significant negative JJA SW-JJA T_s relationship, with a corresponding field significance of 99% for all four reanalyses.

[25] One disadvantage to the above correlation analysis is that it does not reveal simultaneous spatiotemporal variations common to all hydrological variables of interest. In order to identify simultaneous patterns of variation between multiple fields, a multivariate principal component analysis (PCA) was performed on all of the variables shown in Figure 5. Figure 6 shows the resulting empirical orthogonal functions for the second principal component, which accounts for 8% of the joint (standardized) variance (the first component, not shown, accounts for 15%). Over eastern Siberia, this mode is associated with similar signed variations of all seven variables. Figure 6a shows that high ESB snow cover in the prior October is associated with high JFM SWE through much of Asia, including eastern Siberia. Figures 6b, 6c, and 6c show a strong ESB relationship between JFM SWE, JJA SW, JJA ET, and JJA RR. This supports the notion high winter ESB snow mass is associated with high ESB summertime soil moisture, which is sustained through an evaporation-convection feedback (high ET and RR). Although the mode is weakly associated with positive ESB SCA anomalies in October, the relationship with October snow rate is stronger. Moreover, Figure 6g shows that this mode is associated with high ESB SCA in both the current and previous October, and this area closely coincides with the area of ESB October SCA persistence (Figure 4). This pattern of variability further supports the notion that quasi-biennial persistence of October ESB SCA is related to soil moisture anomalies and the evaporation-convection feedback.

[26] A remaining question exists: why is the snow-hydrological feedback strongest in eastern Siberia? One possibility relates to topography: eastern Siberia is more mountainous than western Siberia, which could enhance local precipitation, as well as delay snowmelt until late spring/early summer. A stronger ESB snow-hydrological feedback could also be related to soil type, if a more permeable soil existed in ESB. Although much of Siberia possesses the same soil texture class (i.e., loam), eastern (western) Siberia possesses a bit more silty (sandy) loam [*Rodell et al.*, 2004]. This actually suggests less meltwater infiltration in eastern Siberia, which is consistent with the weaker ESB JFM SWE-JJA SW relationship (Figure 5). Because of the lack of a strong soil type difference across Siberia, and the significant JFM SWE-JJA SW correlations across nearly all of Asia, we favor an alternate explanation involving the seasonal cycle of snow. Figure 7 shows climatological maps of late spring/early summer NOAA snow cover fraction, VIC snowmelt (SM), and VIC 1 m soil water difference (ΔSW) from the prior month. As shown by *Shinoda et al.* [2001], snow first disappears across the Asian continent in the west (during March/April) and then later in the central and east (during May/June). This leads to a similar west-to-east delay in the resulting soil moisture signal, which peaks in April/May in the west and in May/June in the central and east. This is consistent with the observation-based study of *Shinoda* [2001], where most of the snowmelt-soil moisture signal in the west (north of the Caspian and Aral seas) disappeared by May. In north central and eastern Siberia, however, snowmelt and the subsequent soil moisture anomaly are delayed by ~1 month. This delayed seasonal cycle favors a snowmelt-soil water signal in summer (late summer dur-

Table 3. Eastern Siberia Area-Weighted Percentage of Significant Positive (P) and Negative (N) Seasonal Hydrological Correlations Based on the Four Major Reanalyses[a]

	R1		R2		ERA-40		JRA-25	
	P	N	P	N	P	N	P	N
JFM SWE/JJA SW	3.3	**7.1***	1.9	3	4.1	2.9	1.9	1.4
MAM SWE/JJA SW	**6.6***	3.3	**6.4***	1.5	3.8	**4.6**	1.5	3.3
JJA SW/JJA T_s	0.0	**23.6****	0.0	**24.7****	0.4	**28.6****	0.8	**18.0****
JJA SW/SON SWE	**5.2**	4.4	1.0	2.5	2.7	2.9	4.1	0.0

[a]Soil water correlations are based on a 1-meter soil layer depth. Correlations are estimated over the common time period of 1982–2001. Field significance based on resampling is denoted by bold; values without an asterisk are ≥90%; those with one asterisk (*) are ≥95%, and those with two asterisks (**) are ≥99%.

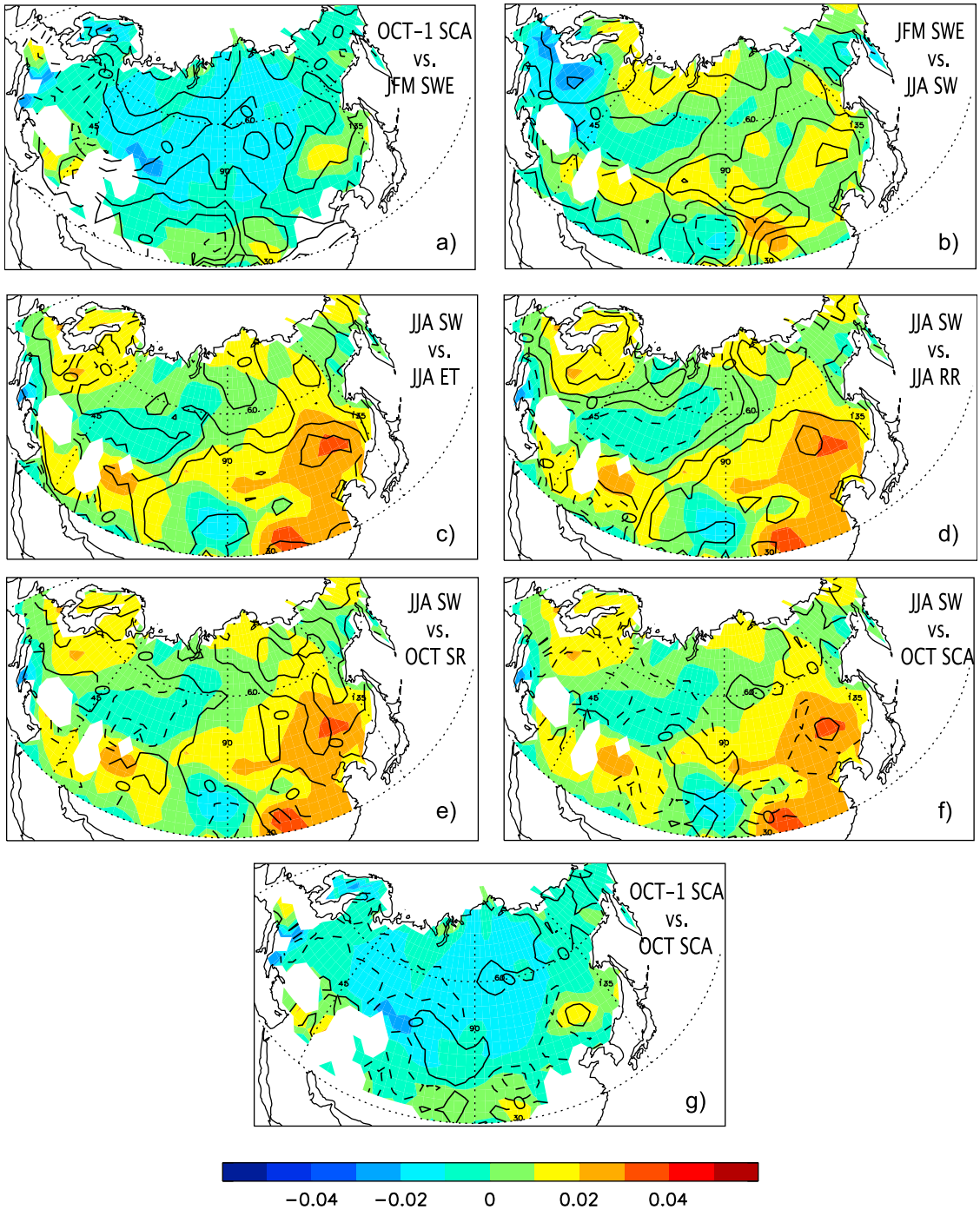

Figure 6. As in Figure 5, but showing the second empirical orthogonal function based on a simultaneous principal component analysis of all indicated fields. The mode accounts for 8% of the joint variance. The contour line interval is identical to color shading interval, with the zero contour line labeled. In each panel, the first quantity is denoted by color shading, and the second quantity is denoted by contour lines (e.g., for JJA SW versus JJA ET, color shading is for JJA SW and contour lines are for JJA ET).

ing high snow years), which in turn favors snow in the early fall (Figure 5). Although VIC shows a stronger JFM SWE-JJA SW relationship in the west (Figure 5), eastern Siberia possesses ~20% more soil water in JJA (on average), consistent with the delayed snowmelt. Moreover, the regions where snow cover lasts through May/June, as well as the resulting SW anomalies, generally correspond to the regions of October snow persistence (Figure 4).

4. Conclusions

[27] The N/AO exhibits preferred periods of low-frequency variability, particularly on the quasi-biennial

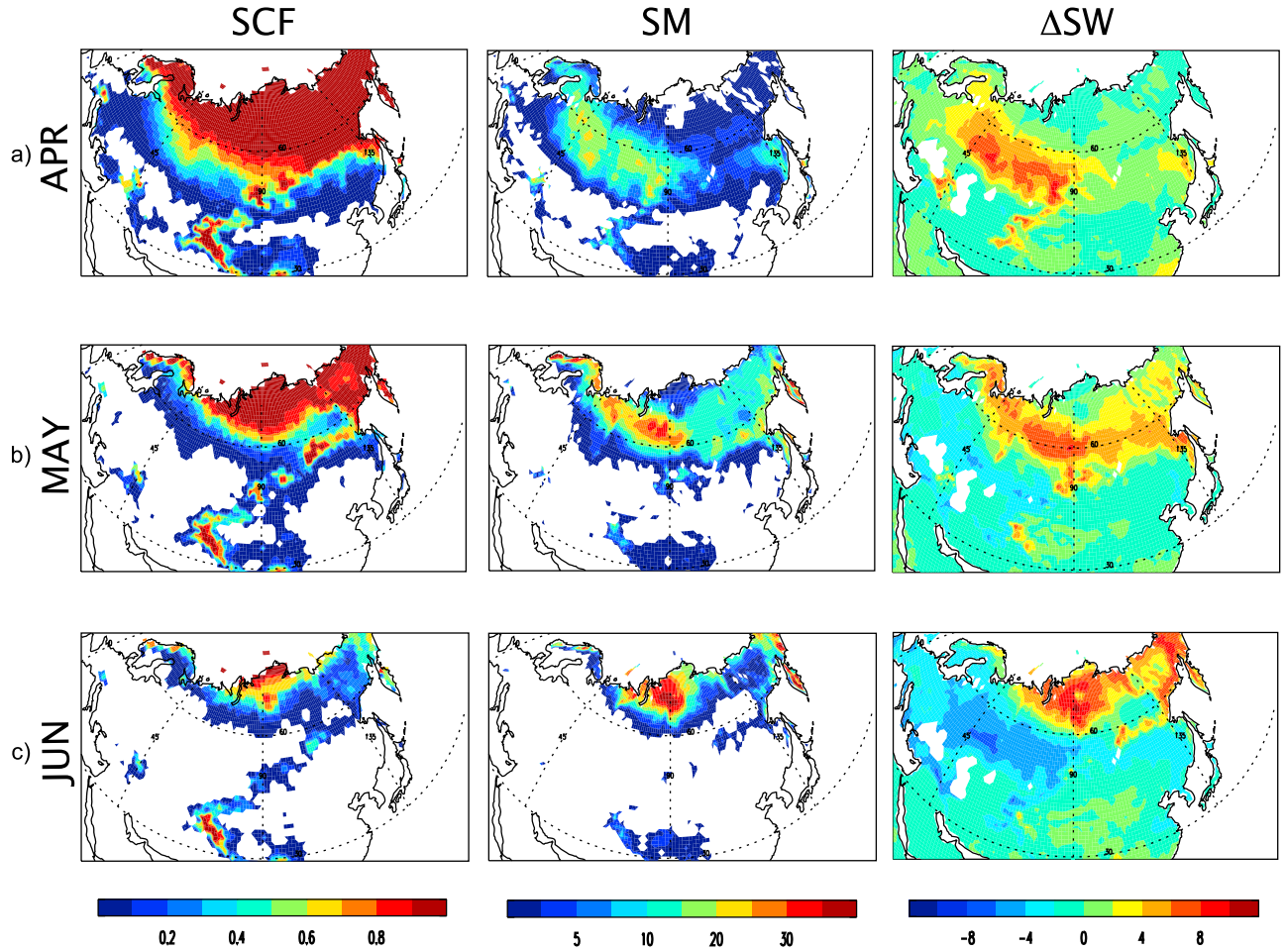

Figure 7. (a) April, (b) May, and (c) June (left) climatological NOAA snow cover fraction (SCF), (middle) VIC snowmelt (SM), and (right) VIC 1 m soil water difference from the prior month (ΔSW). Units ofSM and ΔSW are cm. Zero and nonland values are colored white. April ΔSW is defined as April SW minus March SW and so on.

(2–3 year) timescale [*Schneider and Schonwiese*, 1989; *Stephenson et al.*, 2000; *Cook and D'Arrigo*, 2002; *Saito and Cohen*, 2003]. Similarly, October Eurasian snow cover, especially over eastern Siberia, exhibits quasi-biennial persistence that is strongest in the next 2 years. A snow-AO relationship exists where anomalously high ESB October snow cover increases upward propagating Rossby wave activity, which slows the polar vortex and increases high-latitude geopotential heights, resulting in a negative AO-like response at the surface during winter [*Saito et al.*, 2001; *Cohen et al.*, 2007; *Hardiman et al.*, 2008]. Such a snow-AO relationship, including the upward propagating WAF, increase in ZPC, decrease in U60N, and negative N/AO, exists not only for the subsequent winter, but for the next two to three winters. This suggests the quasi-biennial timescale of the N/AO is related to ESB snow cover anomalies. However, such snow anomalies do not persist through the summer, with most of the snow melting by August. An analysis of the GLDAS land surface models suggests the climate memory of high October ESB snow comes from soil moisture through a snow-hydrological feedback [*Yeh et al.*, 1983; *Yasunari et al.*, 1991]. High winter/spring snow mass is associated with high summertime soil moisture, which in turn is associated with high evapotranspiration and rain rates, and less significantly with lower surface temperatures. This is consistent with the evaporation-convection feedback, which acts to sustain the soil moisture anomaly through the summer, setting the stage for high snow fall rates in the fall when temperatures favor frozen precipitation.

[28] Although October EA SCA has been increasing over the last ~3 decades, springtime EA snow cover has been decreasing. This has been linked to increasing concentrations of GHGs, with a contribution from black carbon aerosols [*Flanner et al.*, 2009]. These trends suggest the snow-hydrological feedback may be weakening, since increased spring snowmelt will reduce the amount of snow persisting to late spring/early summer, weakening the summertime soil moisture anomaly. Thus, the 2–3 year timescale of N/AO variability may likewise weaken. This also implies an increase in year-to-year N/AO variability, which is consistent with observations over the last three decades [*Feldstein*, 2002]. We are currently designing rigorous GCM experiments, and investigating the possibility of using recent, satellite-based observations such as Gravity Recovery and

Climate Experiment (GRACE), to further investigate the snow-hydrological feedback, and its effects on the N/AO.

[29] **Acknowledgments.** This study was funded by NSF grant ARC-0714088 and NASA grant NNX07AR23G, UC Irvine. We thank Min-Hui Lo for useful soil moisture discussions and assisting with the GLDAS data and also two anonymous reviewers. The data used in this study were acquired as part of the mission of NASA's Earth Science Division and are archived and distributed by the Goddard Earth Sciences (GES) Data and Information Services Center (DISC).

References

Allen, R. J., and C. S. Zender (2010), The effects of continental-scale snow albedo anomalies on the wintertime Arctic Oscillation, *J. Geophys. Res.*, *115*, D23105, doi:10.1029/2010JD014490.

Barnett, T. P., L. Dumenil, U. Schlese, and E. Roeckner (1989), The effect of Eurasian snow cover on regional and global climate variations, *J. Atmos. Sci.*, *46*, 661–685.

Berg, A. A., J. S. Famiglietti, M. Rodell, R. H. Reichle, U. Jambor, S. L. Holl, and P. R. Houser (2005), Development of a hydrometeorological forcing data set for global soil moisture estimation, *Int. J. Climatol.*, *25*, 1697–1714.

Bojariu, R., and L. Gimeno (2003), The role of snow cover fluctuations in multiannual NAO persistence, *Geophys. Res. Lett.*, *30*(4), 1156, doi:10.1029/2002GL015651.

Chen, W. Y. (1982), Fluctuations in Northern Hemisphere 700 mb height field associated with the Southern Oscillation, *Mon. Weather Rev.*, *110*, 808–823.

Cohen, J., and M. Barlow (2005), The NAO, the AO and global warming: How closely related?, *J. Clim.*, *18*, 4498–4513.

Cohen, J., and D. Entekhabi (1999), Eurasian snow cover variability and Northern Hemisphere climate predictability, *Geophys. Res. Lett.*, *26*(3), 345–348.

Cohen, J., M. Barlow, P. J. Kushner, and K. Saito (2007), Stratosphere-troposphere coupling and links with Eurasian land surface variability, *J. Clim.*, *20*, 5335–5343.

Cohen, J., J. Foster, M. Barlow, K. Saito, and J. Jones (2010), Winter 2009–2010: A case study of an extreme Arctic Oscillation event, *Geophys. Res. Lett.*, *37*, L17707, doi:10.1029/2010GL044256.

Cook, E. R., and R. D. D'Arrigo (2002), A well-verified, multiproxy reconstruction of the winter North Atlantic Oscillation index since A.D. 1400, *J. Clim.*, *15*, 1754–1764.

Cook, E. R., R. D. D'Arrigo, and K. R. Briffa (1998), A reconstruction of the North Atlantic Oscillation using tree-ring chronologies from North America, *Holocene*, *8*, 9–17.

Dirmeyer, P. A., and K. L. Brubaker (2007), Characterization of the global hydrologic cycle from a back-trajectory analysis of atmospheric water vapor, *J. Hydrometeorol.*, *8*, 20–37.

Dirmeyer, P. A., C. A. Schlosser, and K. L. Brubaker (2009), Precipitation, recycling, and land memory: An integrated analysis, *J. Hydrometeorol.*, *10*, 278–288.

Edmon, H. J., Jr., B. J. Hoskins, and M. E. McIntyre (1980), Eliassen-Palm cross sections for the troposphere, *J. Atmos. Sci.*, *37*, 2600–2616.

Feldstein, S. B. (2000), The timescale, power spectra, and climate noise properties of teleconnection patterns, *J. Clim.*, *13*, 4430–4440.

Feldstein, S. B. (2002), The recent trend and variance increase of the annular mode, *J. Clim.*, *15*, 88–94.

Flanner, M. G., and C. S. Zender (2005), Snowpack radiative heating: Influence on Tibetan Plateau climate, *Geophys. Res. Lett.*, *32*, L06501, doi:10.1029/2004GL022076.

Flanner, M. G., C. S. Zender, P. G. Hess, N. M. Mahowald, T. H. Painter, V. Ramanathan, and P. J. Rasch (2009), Springtime warming and reduced snow cover from carbonaceous particles, *Atmos. Chem. Phys.*, *9*, 2481–2497.

Fletcher, C. G., S. C. Hardiman, P. J. Kushner, and J. Cohen (2009), The dynamical response to snow cover perturbations in a large ensemble of atmospheric GCM integrations, *J. Clim.*, *22*, 1208–1222.

Fyfe, J. C., G. J. Boer, and G. M. Flato (1999), The Arctic and Antarctic Oscillations and their projected changes under global warming, *Geophys. Res. Lett.*, *26*(11), 1601–1604.

Gillett, N. P., F. W. Zwiers, A. J. Weaver, and P. A. Stott (2003), Detection of human influence on sea-level pressure, *Nature*, *422*, 292–294.

Gong, G., D. Entekhabi, and J. Cohen (2002), A large-ensemble model study of the wintertime AO-NAO and the role of interannual snow perturbations, *J. Clim.*, *15*, 3488–3499.

Gong, G., D. Entekhabi, and J. Cohen (2003), Modeled Northern Hemisphere winter climate response to realistic Siberian snow anomalies, *J. Clim.*, *16*, 3917–3931.

Hardiman, S. C., P. J. Kushner, and J. Cohen (2008), Investigating the ability of general circulation models to capture the effects of Eurasian snow cover on winter climate, *J. Geophys. Res.*, *113*, D21123, doi:10.1029/2008JD010623.

Hoerling, M., J. W. Hurrell, and T. Xu (2001), Tropical origins for recent North Atlantic climate change, *Science*, *292*, 90–92.

Hurrell, J. (1995), Decadal trends in the North Atlantic oscillation and relationships to regional temperature and precipitation, *Science*, *269*, 676–679.

Hurrell, J. W., M. P. Hoerling, A. S. Phillips, and T. Xu (2004), Twentieth century North Atlantic climate change. Part I: Assessing determinism, *Clim. Dyn.*, *23*, 371–389.

Jones, P. D., T. J. Osborn, and K. R. Briffa (2001), The evolution of climate over the last millennium, *Science*, *292*, 662–667.

Kalnay, E., et al. (1996), The NCEP/NCAR 40-year reanalysis project, *Bull. Am. Meteorol. Soc.*, *77*, 437–471.

Kanamitsu, M., W. Ebisuzaki, J. Woollen, S.-K. Yang, J. J. Hnilo, M. Fiorino, and G. L. Potter (2002), NCEP-DOE AMIP-II Reanalysis (R-2), *Bull. Am. Meteorol. Soc.*, *83*, 1631–1643.

Li, H., A. Robock, S. Liu, X. Mo, and P. Viterbo (2005), Evaluation of reanalysis soil moisture simulations using updated Chinese soil moisture observations, *J. Hydrometeorol.*, *6*, 180–193.

Livezey, R. E. (1999), Field intercomparison, in *Analysis of Climate Variability: Applications of Statistical Techniques*, pp. 159–175, Springer, Berlin.

Lu, C.-H., M. Kanamitsu, J. O. Roads, W. Ebisuzaki, K. E. Mitchell, and D. Lohmann (2005), Evaluation of soil moisture in the NCEP-NCAR and NCEP-DOE global reanalyses, *J. Hydrometeorol.*, *6*, 391–408.

Matsumura, S., K. Yamazaki, and T. Tokioka (2010), Summertime land-atmosphere interactions in response to anomalous springtime snow cover in northern Eurasia, *J. Geophys. Res.*, *115*, D20107, doi:10.1029/2009JD012342.

Miller, R. L., G. A. Schmidt, and D. T. Shindell (2006), Forced annular variations in the 20th century Intergovernmental Panel on Climate Change Fourth Assessment Report models, *J. Geophys. Res.*, *111*, D18101, doi:10.1029/2005JD006323.

Onogi, K., et al. (2007), The JRA-25 reanalysis, *J. Meteorol. Soc. Jpn.*, *85*, 369–432.

Osborn, T. J. (2004), Simulating the winter North Atlantic Oscillation: The roles of internal variability and greenhouse gas forcing, *Clim. Dyn.*, *22*, 605–623.

Plumb, R. A. (1985), On the three-dimensional propagation of stationary waves, *J. Atmos. Sci.*, *42*, 217–229.

Ringler, T. D., and K. H. Cook (1999), Understanding the seasonality of orographically forced waves: Interaction between mechanical and thermal forcing, *J. Atmos. Sci.*, *56*, 1154–1174.

Robertson, A. W., C. R. Mechoso, and Y.-J. Kim (2000), The influence of Atlantic sea surface temperature anomalies on the North Atlantic Oscillation, *J. Clim.*, *13*, 122–138.

Robock, A., K. Vinnikov, G. Srinivasan, J. Entin, S. Hollinger, N. Speranskaya, S. Liu, and A. Namkhai (2000), The Global Soil Moisture Data Bank, *Bull. Am. Meteorol. Soc.*, *81*(6), 1281–1299.

Rodell, M., et al. (2004), The Global Land Data Assimilation System, *Bull. Am. Meteorol. Soc.*, *85*, 381–394.

Rodwell, M. J., D. P. Rowell, and C. K. Folland (1999), Oceanic forcing of the wintertime North Atlantic Oscillation and European climate, *Nature*, *398*, 320–323.

Rogers, J. C. (1984), The association between the North Atlantic Oscillation and the Southern Oscillation in the Northern Hemisphere, *Mon. Weather Rev.*, *112*, 1999–2015.

Saito, K., and J. Cohen (2003), The potential role of snow cover in forcing interannual variability of the major Northern Hemisphere mode, *Geophys. Res. Lett.*, *30*(6), 1302, doi:10.1029/2002GL016341.

Saito, K., J. Cohen, and D. Entekhabi (2001), Evolution of atmospheric response to early-season Eurasian snow cover anomalies, *Mon. Weather Rev.*, *129*, 2746–2760.

Schneider, U., and C.-D. Schonwiese (1989), Some statistical characteristics of El Nino/Southern Oscillation and North Atlantic Oscillation indices, *Atmosfera*, *2*, 167–180.

Shindell, D. T., R. L. Miller, G. A. Schmidt, and L. Pandolfo (1999), Simulation of recent northern winter climate trends by greenhouse-gas forcing, *Nature*, *399*, 452–455.

Shinoda, M. (2001), Climate memory of snow mass as soil moisture over central Eurasia, *J. Geophys. Res.*, *106*(D24), 33,393–33,403.

Shinoda, M., H. Utsugi, and W. Morishima (2001), Spring snow-disappearance timing and its possible influence on temperature fields over central Eurasia, *J. Meteorol. Soc. Jpn.*, *79*, 37–59.

Stephenson, D. B., V. Pavan, and R. Bojariu (2000), Is the North Atlantic Oscillation a random walk?, *Int. J. Climatol.*, *20*, 1–18.

Thompson, D. W. J., and J. M. Wallace (1998), The Arctic Oscillation signature in the wintertime geopotential height and temperature fields, *Geophys. Res. Lett.*, *25*(9), 1297–1300.

Thompson, D. W. J., and J. M. Wallace (2000), Annular modes in the extratropical circulation. Part I: Month to month variability, *J. Clim.*, *13*, 1000–1016.

Uppala, S., et al. (2005), The ERA-40 re-analysis, *Q. J. R. Meteorol. Soc.*, *131*, 2961–3012.

van der Ent, R. J., H. H. G. Savenije, B. Schaefli, and S. C. Steele-Dunne (2010), Origin and fate of atmospheric moisture over continents, *Water Resour. Res.*, *46*, W09525, doi:10.1029/2010WR009127.

Wallace, J. M., and D. S. Gutzler (1981), Teleconnections in the geopotential height field during the Northern Hemisphere winter, *Mon. Weather Rev.*, *109*, 784–812.

Wilks, D. S. (1995), *Statistical Methods in the Atmospheric Sciences*, 467 pp., Academic, San Diego, Calif.

Yasunari, T., A. Kitoh, and T. Tokioka (1991), Local and remote responses to excessive snow mass over Eurasia appearing in the northern spring and summer climate—A study with the MRI GCM, *J. Meteorol. Soc. Jpn.*, *69*, 473–487.

Ye, H. (2001), Quasi-biennial and quasi-decadal variations in snow accumulation over northern Eurasia and their connections to the Atlantic and Pacific oceans, *J. Clim.*, *14*, 4573–4584.

Yeh, T.-C., R. T. Wetherald, and S. Manabe (1983), A model study of the short-term climatic and hydrologic effects of sudden snow-cover removal, *Mon. Weather Rev.*, *111*, 1013–1024.

Zhang, J., W.-C. Wang, and J. Wei (2008), Assessing land-atmosphere coupling using soil moisture from the Global Land Data Assimilation System and observational precipitation, *J. Geophys. Res.*, *113*, D17119, doi:10.1029/2008JD009807.

R. J. Allen and C. S. Zender, Department of Earth System Science, University of California, Irvine, CA 92697, USA. (rjallen@uci.edu)